https://doi.org/10.1016/j.ijleo.2019.164112

Design and simulation of a high efficiency CdS/CdTe solar cell

I. E. Tinedert[1], F. Pezzimenti[2,*], M. L. Megherbi[1], and A. Saadoune[1]

[1] LMSM – Mohammed Khieder University, 07000 Biskra, Algeria.

[2] DIIES – Mediterranea University of Reggio Calabria, 89100 Reggio Calabria, Italy.

[*]Corresponding author: fortunato.pezzimenti@unirc.it

Abstract: A thin film solar cell based on cadmium telluride (CdTe) has been investigated by means of an accurate numerical simulation study. To optimize the design in terms of power conversion efficiency, we have studied the influence of doping concentration and carrier lifetime in the CdTe layer as well as the impact of different geometrical parameters in defining the device structure. In more detail, the solar cell consists of a fluorine doped tin oxide layer stacked, from top to bottom, on a highly resistive transparent film, a n-type layer of cadmium sulphide (CdS), and a p-type CdTe absorber layer. A good agreement between the simulation results and recent experimental data taken from literature has been achieved. The optimized design performs a short-circuit current density of 29.09 mA/cm^2, an open-circuit voltage of 0.95 V, a fill-factor of 83.47%, and a conversion efficiency on the order of 23% under air mass 1.5 global spectrum (AM1.5G) with an incident irradiance of 1000 W/m^2.

Keywords: CdTe solar cell; numerical simulations; fill-factor; conversion efficiency.

1. Introduction

In the last decade, the use of cadmium telluride (CdTe) in the field of high efficiency solar cells developed meaningfully. In fact, thanks to the material long-term stability and low cost, CdTe appeared promising for the manufacture of solar cells able to absorb wavelengths typically between 350 nm and 850 nm. Conversion efficiencies on the order of 20% with low energy costs (~0.0387 $/kWh) were already demonstrated experimentally [1,2].

CdTe is from group II-VI of compound polycrystalline semiconductors with a direct optical bandgap close to 1.5 eV, which makes it well suited for energy conversion in photovoltaic. At the same time, by

https://doi.org/10.1016/j.ijleo.2019.164112

considering the material high absorption coefficient (5×10^5 cm^{-1}), a 2-μm-thick p-type substrate could be enough to absorb the sun beams [3]. However, solar cells are manufactured with a CdTe thickness ranging from 4 μm to 6 μm for a better performance [4].

In a CdTe-based device, cadmium sulphide (CdS) is a good candidate to form a p-n junction which enables the photovoltaic effect. The bandgap of CdS is 2.42 eV and this value corresponds to an absorption edge close to 500 nm [5,6]. For commercial purpose, CdS/CdTe solar cells are usually deposited on a glass substrate coated with a transparent conducting oxide (TCO) which consists, for example, of fluorine-doped tin oxide (SnO_2:F or FTO). In addition, to increase the cell efficiency limiting the effect of non-uniformities, a high-resistive transparent (HRT) thin film, e.g. moderate doped SnO_2, is placed between the TCO and the CdS regions [7,8]. This layer has a negligible effect on the spectral response of the cell and in practice it acts as a buffer layer.

In this work, we used the Silvaco-Atlas simulation software [9] to investigate and optimize the electrical characteristics of a CdS/CdTe solar cell. Firstly, the measurements reported in Ref. [10] were fitted to validate the numerical models taken into account. Then, in order to obtain an improved performance we evaluated the impact of the fundamental geometrical and physical parameters in the different device regions in determining the overall solar cell conversion efficiency. Recent manuscripts of ours, which are focused on the modelling of different photovoltaic devices, support the adopted simulation setup [11-18].

The optimized design, with a 0.4-μm-thick FTO and 0.1-μm-thick CdS layer (window layer), exhibits a conversion efficiency in excess of 23% at room temperature. Air mass 1.5 global spectrum (AM1.5G) with an incident irradiance of 1000 W/m^2 was assumed during the simulations. The obtained results represent a significant improvement with respect to the performance reported in Ref. [10] which is close to 14%, and they could turn useful for the design and realization of high efficiency CdTe-based solar cells with saving time and money.

2. Cell structure

The considered device structure is schematized in Fig. 1. Basically, it consists of a CdS(n)/CdTe(p) heterojunction with a n-type and p-type doping concentration of 1×10^{18} cm^{-3} and 2×10^{14} cm^{-3},

https://doi.org/10.1016/j.ijleo.2019.164112

respectively. A transparent film of SnO_2 acts as HRT layer between the TCO and the CdS regions. A deposition of a 5nm/50nm of Cu/Au forms the back contact. Details about the fabrication process are reported in Ref. [10].

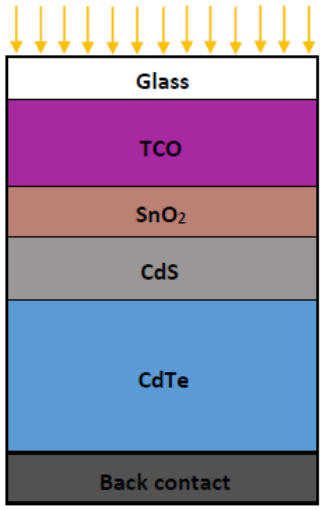

Fig. 1. CdS/CdTe solar cell.

The device geometrical and physical parameters are listed in Table 1. For simulation purposes, the glass/TCO substrate was modelled as a FTO layer with a thickness of 400 nm and a n-type doping concentration of 3×10^{20} cm^{-3}.

Table 1. Device parameters.

	Layers			
	FTO	SnO_2	CdS	CdTe
Thickness (μm)	0.4	0.1	0.1	6
Bandgap energy, E_g (eV)	3.6	3.6	2.42	1.5
Electron affinity (eV)	4.5	4.5	4.3	4.28
Dielectric ratio	9	9	10	9.4
N-type doping, N_d (cm^{-3})	3×10^{20}	1×10^{18}	1×10^{18}	-
P-type doping, N_a (cm^{-3})	-	-	-	2×10^{14}

3. Simulation setup

During the simulations, the key physical models taken into account included the Shockley-Read-Hall (SRH) and radiative recombination processes, the bandgap narrowing (BGN) effect, and the doping-dependent carrier mobility and carrier lifetime. In more detail, the effective carrier concentration in each device region was calculated in the form

https://doi.org/10.1016/j.ijleo.2019.164112

$$n_{ie}^2 = n_i^2 exp\left(\frac{\Delta E_g}{kT}\right) \quad (1)$$

where k is Boltzmann's constant, T is the temperature, ΔE_g is the bandgap due to the BGN effect [19,20], and n_i is the intrinsic concentration of carriers depending on E_g and the carrier density of states in the conduction (N_c) and valence (N_v) band:

$$n_i = \sqrt{N_c N_v} exp\left(-\frac{E_g}{2kT}\right). \quad (2)$$

To describe the carrier behaviour at the thermal equilibrium we used the Fermi-Dirac statistics defined by the relation [21]

$$f(\epsilon) = \frac{1}{1+exp\left(\frac{\epsilon - E_F}{KT}\right)} \quad (3)$$

where $f(\varepsilon)$ is the energy level occupation probability for electrons and E_F is the Fermi level.

The recombination phenomena were modelled by means of the SRH expression as follows [22-24]:

$$R_{SRH} = \frac{pn - n_i^2}{\tau_n\left[n + n_{ie} exp\left(\frac{E_{TRAP}}{KT}\right)\right] + \tau_P\left[p + n_{ie} exp\left(\frac{-E_{TRAP}}{KT}\right)\right]} \quad (4)$$

where E_{TRAP} is the difference between the trap energy level and the intrinsic Fermi level, and τ_n, τ_p are the carrier lifetime for electrons and holes, respectively. In addition, the radiative (optical) recombination process was described by the standard relation [25,26]

$$U_r = B_r\left(np - n_i^2\right) \quad (5)$$

where B_r is the radiative recombination coefficient assumed equal to 4.72×10^{-11} cm^3/s [27]. The effective carrier lifetimes in the different device regions was therefore imposed through the expression [28]

$$\frac{1}{\tau_{n,p}} = \frac{1}{\tau_{NRn,p}} + B_r \times N \quad (6)$$

where $\tau_{NRn,p}$ is the non-radiative contribution and N is the total (local) doping concentration.

Finally, to describe the doping-dependent carrier mobility, a simplified low-field mobility model was used in the form of [29-31]

https://doi.org/10.1016/j.ijleo.2019.164112

$$\mu_{n,p} = \frac{\mu_{0n,p}}{1+\left(\frac{N}{N_{n,p}^{crit}}\right)^{\delta_{n,p}}} \tag{7}$$

where $\mu_{0n,p}$, $N_{n,p}^{crit}$, and $\delta_{n,p}$ are reference constants.

The fundamental simulation parameters used as entry data in this study are summarized in Table 2. These values are consistent with recent literature on CdS/CdTe solar cells [32-36]. In particular, the carrier lifetimes in the CdTe region were fixed to 1 ns, though values up to 10 ns could be considered for a low defect material [37,38].

Table 2. Simulation parameters.

	Layers			
	FTO	SnO_2	CdS	CdTe
N_v (cm^{-3})	1.8×10^{19}	1.8×10^{19}	1.8×10^{19}	1.8×10^{19}
N_c (cm^{-3})	2.2×10^{18}	2.2×10^{18}	2.2×10^{18}	8×10^{17}
μ_{0n} (cm^2/Vs)	100	100	100	320
μ_{0p} (cm^2/Vs)	25	25	25	60
τ_{NRn} (ns)	100	100	0.01	1
τ_{NRp} (ns)	0.1	0.1	0.01	1

4. Results and discussion

During the simulations, the device active area was 0.25 cm^2 and it was illuminated with an incident irradiance of 1000 W/m^2. Firstly, to validate the assumed simulation models and parameters, the solar cell current density-voltage (J-V) experimental curve reported in Ref. [10] was fitted as shown in Fig. 2.

The experimental and simulated behaviours appear in good agreement in the whole considered voltage range. The main photovoltaic parameters extracted from Fig. 2, namely the short-circuit current density (J_{sc}), open circuit voltage (V_{oc}), fill factor (FF), and conversion efficiency (η), are listed in Table 3. These results support the simulation analysis and highlight that the reference structure in Table 1 performs an overall conversion efficiency of 14%.

https://doi.org/10.1016/j.ijleo.2019.164112

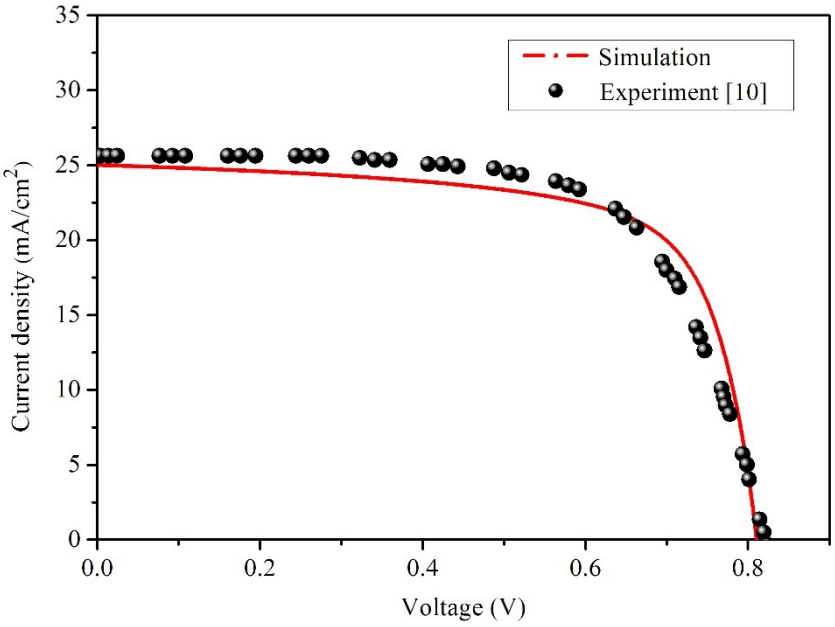

Fig. 2. J-V curve of the considered CdS/CdTe solar cell.

Table 3. Photovoltaic parameters for the reference device.

	J_{sc} (mA/cm^2)	V_{oc} (V)	FF (%)	η (%)
Simulation	25.01	0.81	69.89	14.16
Experiment [10]	25.6	0.82	66.4	14

4.1. Effect of the CdTe absorber layer

By assuming an increasing value of the acceptor doping concentration in the CdTe region, the cell performance in terms of η improves as shown in Fig. 3. In particular, starting from $N_a = 2\times10^{14}$ cm^{-3} (reference value in Table 1), the cell efficiency increases rapidly up to about 16.9%.

The effect of the CdTe layer thickness was also investigated as shown in Fig. 4. Here, a fixed doping concentration of 2×10^{15} cm^{-3} was considered.

CdTe thicknesses lower than 2 μm strongly penalize the solar cell efficiency. At the same time, a thicker absorber layer allows, in principle, a better performance. This improvement, however, appears rather limited.

https://doi.org/10.1016/j.ijleo.2019.164112

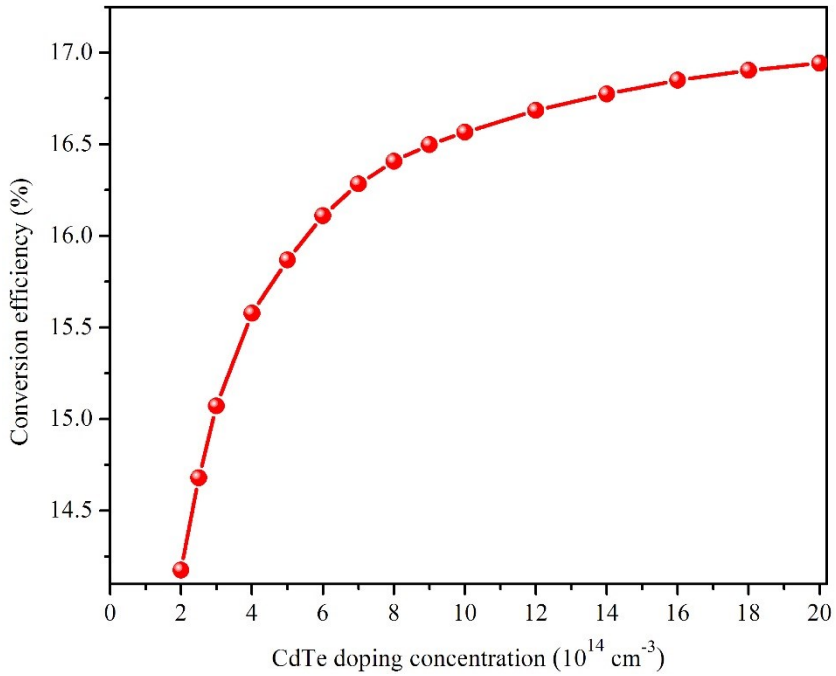

Fig. 3. Cell efficiency as a function of the doping concentration in the CdTe region.

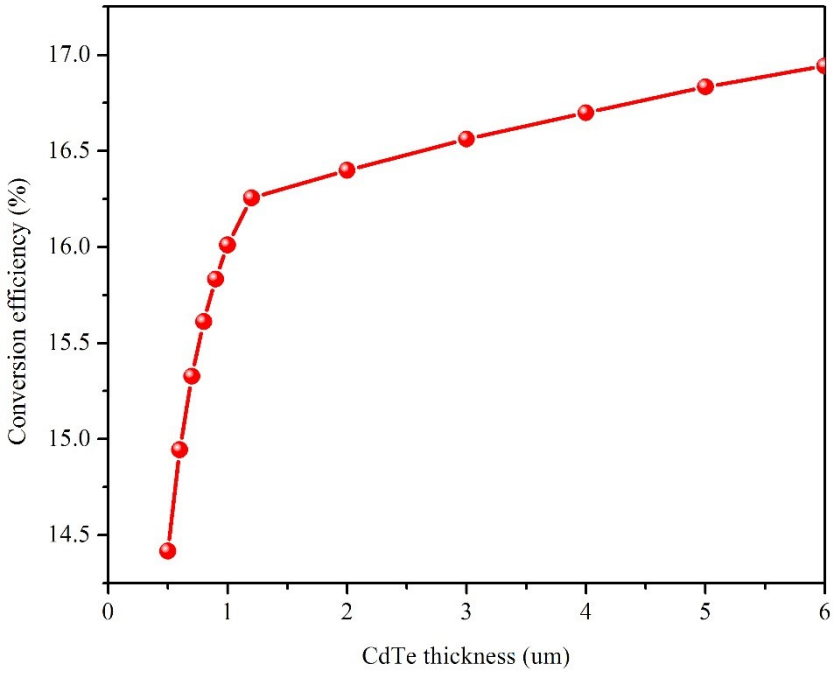

Fig. 4. Cell efficiency as a function of the CdTe layer thickness.

4.2. Effect of the CdS window layer

Starting from an optimized 6-µm thick CdTe substrate with $N_a = 2\times10^{15}$ cm^{-3}, the CdS window layer impact on the cell efficiency was evaluated for different donor doping concentrations and

https://doi.org/10.1016/j.ijleo.2019.164112

thicknesses. In more detail, in Fig. 5 is shown the η behaviour for a thickness of 100 nm and N_d ranging from 1×10^{17} cm^{-3} to 1×10^{19} cm^{-3}. As we can see, $N_d = 1\times10^{18}$ cm^{-3} (reference value in Table 1) appears as an optimal value which determines an efficiency peak close to 16.94%.

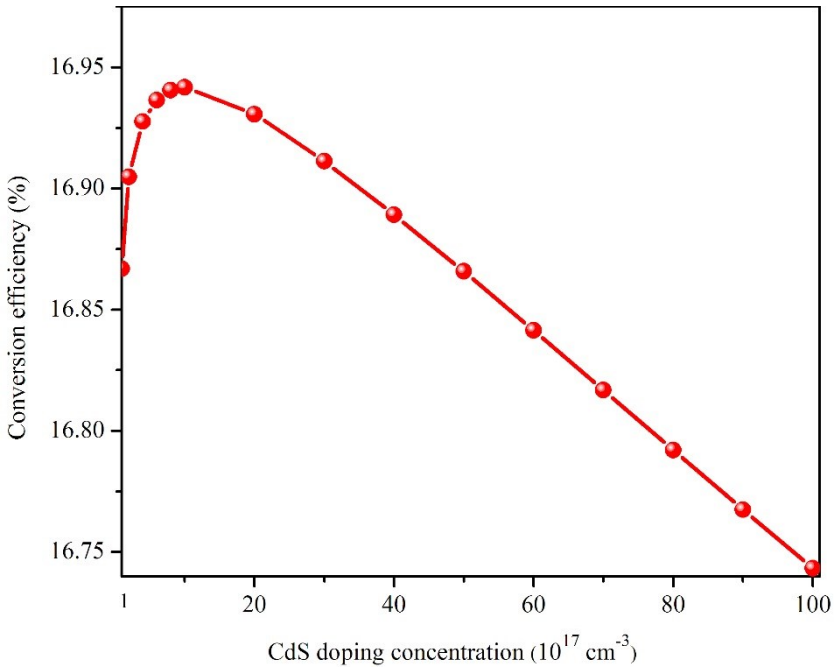

Fig. 5. Cell efficiency as a function of the doping concentration in the CdS region.

For $N_d = 1\times10^{18}$ cm^{-3}, different thicknesses of the CdS region were considered between 20 nm and 100 nm as shown in Fig. 6. The CdS thickness determines, de facto, the effective light transmittance to the CdTe layer.

Although the cell efficiency tends to increase for thinner CdS regions, thicknesses below 50 nm are considered not electrically reliable resulting, in fact, discontinuous and shorting the cell [38]. For a thickness of 50 nm we achieve an efficiency as high as 18.5%.

https://doi.org/10.1016/j.ijleo.2019.164112

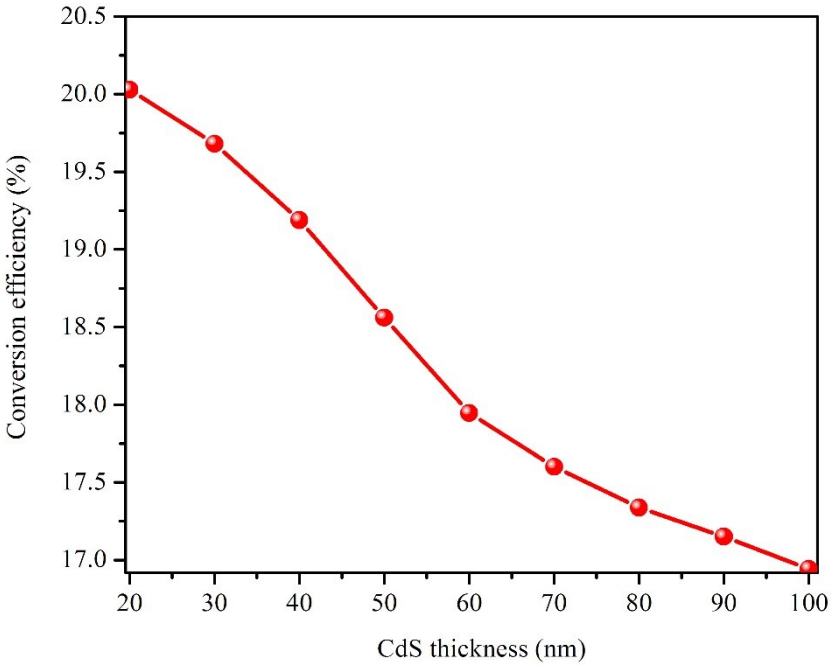

Fig. 6. Cell efficiency as a function of the CdS layer thickness.

4.3. Optimized design

Together with the presented analysis on the role of the CdTe and CdS layers, further investigations have been made considering different thicknesses of the SnO_2 region in the range 50-120 nm. The simulations showed that this parameter has only a limited impact on the cell performance and the conversion efficiency has a variation in the limit of 2%.

The comparison between the simulated J–V characteristics of the reference cell in Table 1 and the improved design obtained by combining the previous results in terms of doping concentrations and geometrical parameters is shown in Fig. 7. Here, the J-V curve of an optimized device, where a longer carrier lifetime of 10 ns is imposed for electrons and holes in the CdTe region, is also reported. This value, in fact, is suggested in Refs. [36] and [37] as well appropriate for high-purity CdTe-based solar cells in dependence of their fabrication process.

In more detail, the cell efficiency behaviour calculated as a function of the carrier lifetimes in the CdTe absorber layer is shown in Fig. 8. As expected, the decrease of the recombination phenomena in the space-charge region of the CdS/CdTe heterojunction leads to an increased efficiency which is calculated on the order of 23%.

https://doi.org/10.1016/j.ijleo.2019.164112

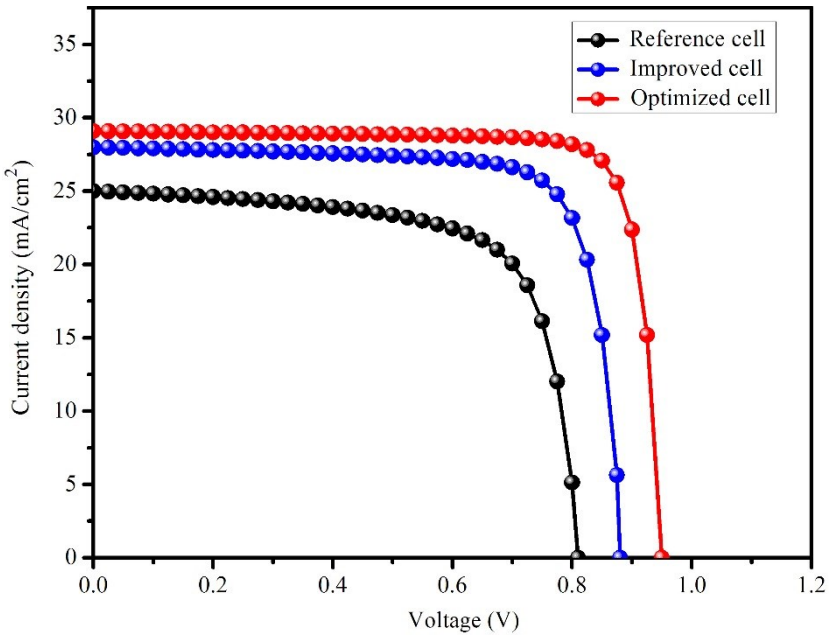

Fig. 7. J-V characteristics of different designs.

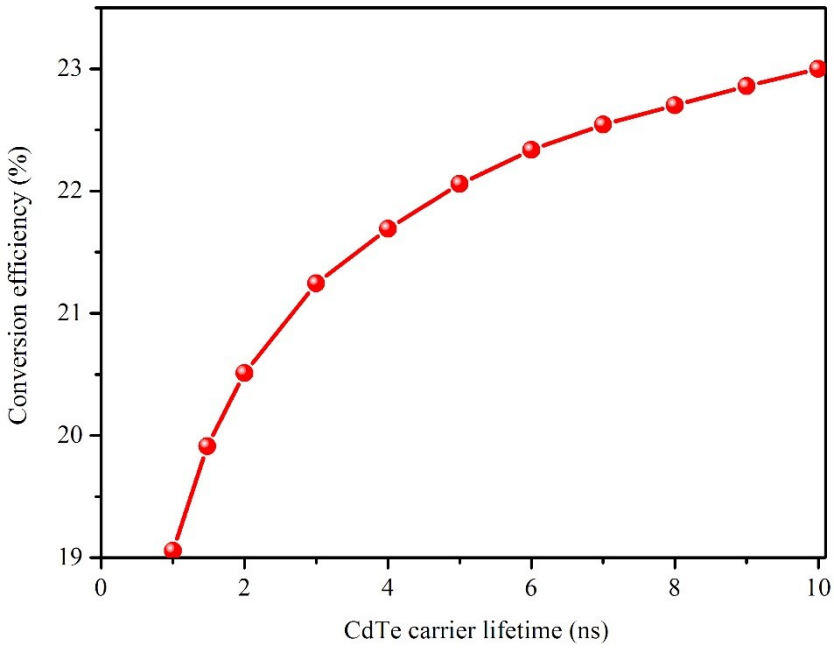

Fig. 8. Cell efficiency as a function of the carrier lifetime in the CdTe absorber layer.

The photovoltaic parameters extracted from Fig. 7 are summarized in Table 4.

https://doi.org/10.1016/j.ijleo.2019.164112

Table 4. Photovoltaic parameters.

	J_{sc} (mA/cm^2)	V_{oc} (V)	FF (%)	η (%)
Reference cell	25.01	0.81	69.89	14.16
Improved cell	28.01	0.87	78.08	19.02
Optimized cell with longer carrier lifetime	29.09	0.95	83.47	23.01

Compared to the reference device, the improved cell is based on a CdTe substrate with an acceptor doping concentration of 2×10^{15} cm^{-3} and the CdS and SnO_2 thicknesses both scaled to 50 nm. It performs an overall conversion efficiency of 19.02%. This result could be further optimized up to a value of 23.01% by considering a longer carrier lifetime (10 ns) in the CdTe region.

4.4. Spectral response

The useful wavelength range of the investigated solar cell can be observed by plotting the device external quantum efficiency (EQE). This figure of merit is defined as the ratio between the effective photocurrent calculated through the cell and the source photocurrent which is in the form of [9]

$$Isrc = \frac{1}{hc} q\lambda P_b W_b \tag{8}$$

where λ is the photon wavelength, q is the electronic charge, c is the speed of light, h is Planck's constant, P_B is the power density of the incident light, and W_B is the beam width clipped to the device.

For a given light source, the available photocurrent through the cell depends on the optical properties of the different materials. In particular, the wavelength-dependent refractive index (n) and extinction coefficient (k) of the CdS and CdTe layers have been assumed according to [39] where they were extracted experimentally in the 250-1500 nm wavelength range. At the same time, we referred to [38] to characterize the SnO_2 region optically.

The EQE behaviour of the reference and optimized cell in Table 4 are shown in Fig. 9 for a wavelength range extending from 300 nm to 950 nm.

For the optimized design, we can observe an increased EQE in the whole explored wavelength range before the CdTe optical bandgap determines an absorption edge close to 850 nm. The maximum absorption occurs in the range $500 < \lambda < 800$ nm where the average EQE is on the order of 96% with a

https://doi.org/10.1016/j.ijleo.2019.164112

maximum of 96.98% at λ = 650 nm. The absorption knee around λ = 500 nm is due to the CdS material properties. Finally, below this λ value the light is mainly absorbed by the FTO layer.

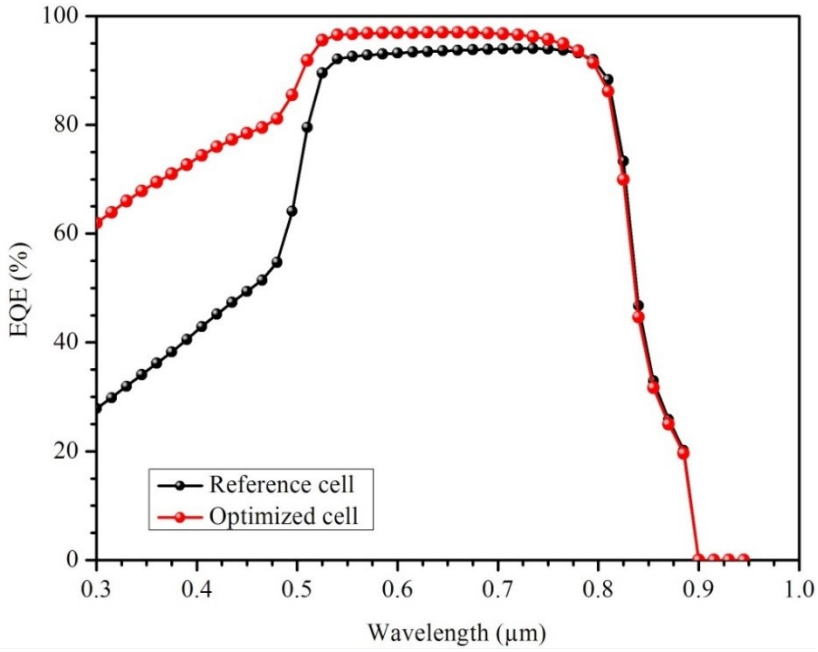

Fig. 9. External quantum efficiency behaviours.

Conclusion

The fundamental photovoltaic parameters of different solar cells based on the CdS/CdTe heterojunction were calculated. The role of the doping concentration and thickness of both the CdS and CdTe region in determining the device performance was investigated by means of a careful numerical simulation analysis.

The simulation results for the reference cell are in good agreement with the experimental data reported in literature. The optimized design performs a high short circuit current density of 29.09 mA/cm^2, an open circuit voltage of 0.95 V, and a fill-factor of 83.47%. The conversion efficiency is 23.01%. This value appears strongly dependent on the CdTe thickness and carrier lifetime.

References

[1] M.A. Green, Y. Hishikawa, E.D. Dunlop, D.H. Levi, J. Hohl-Ebinger, M. Yoshita, A.W.Y. Ho-Baillie, Solar cell efficiency tables (ver, 53), Prog. Photovolt. Res. Appl. 27 (2019) 3-12.

[2] D.E. Swanson, J.R. Sites, W.S. Sampath, Co-sublimation of $CdSe_X$ Te_{1-X} layers for CdTe solar cells, Sol. Energ. Mat. Sol. C. 159 (2017) 389-394.

[3] X. Wu, High-efficiency polycrystalline CdTe thin-film solar cells, Sol. Energy 77 (2004) 803-814.

[4] A. Romeo, M. Terheggen, D. Abou-Ras, D.L. Bätzner, F.J. Haug, M. Kälin, D. Rudmann, A.N. Tiwari, Development of thin-film Cu(In,Ga)Se2 and CdTe solar cells, Prog. Photovolt. Res. Appl. 12 (2004) 93-111.

[5] J. Lee, Comparison of CdS films deposited by different techniques: Effects on CdTe solar cell, Appl. Surf. Sci. 252 (2005) 1398-1403.

[6] J. Britt, C. Ferekides, Thin-film CdS/CdTe solar cell with 15.8% efficiency, Appl. Phys. Lett. 62 (1993) 2851-2852.

[7] S.D. Feldman, L. Mansfield, T.R. Ohno, V. Kaydanov, J.D. Beach, T. Nagle, Non-uniformity mitigation in CdTe solar cells: The effects of high-resistance transparent conducting oxide buffer layers, in Conference Record of the Thirty-first IEEE photovoltaic Specialists Conference (2005) 271-274.

[8] H. Mahabaduge, K. Wieland, C. Carter, V. Plotnikov, D. Giolando, Sputtered HRT layers for CdTe solar cells, in Proc. IEEE 37th Photovoltaic Specialists Conference (2011) 001302-001304.

[9] Silvaco Atlas User's Manual Device Simulation Software. Santa Clara, CA, 2016.

[10] T. Baines, G. Zoppi, L. Bowen, T.P. Shalvey, S. Mariotti, Incorporation of CdSe layers into CdTe thin film solar cells, Sol. Energ. Mat. Sol. C. 180 (2018) 196-204.

[11] H. Bencherif, L. Dehimi, F. Pezzimenti, F.G. Della Corte, Improving the efficiency of a-Si:H/c-Si thin heterojunction solar cells by using both antireflection coating engineering and diffraction grating, Optik 182 (2019) 682-693.

[12] F. Bouzid, L. Dehimi, F. Pezzimenti, M. Hadjab, A.H. Larbi, Numerical simulation study of a high efficiency AlGaN-based ultraviolet photodetector, Superlattice. Microst. 122 (2018) 57-73.

[13] Y. Marouf, L. Dehimi, F. Bouzid, F. Pezzimenti, F.G. Della Corte, Theoretical design and performance of $In_xGa_{1-x}N$ single junction solar cell, Optik 163 (2018) 22-32.

[14] F. Bouzid, L. Dehimi, F. Pezzimenti, Performance Analysis of a Pt/n-GaN Schottky barrier UV detector, J. Electron Mater. 46 (2017) 6563-6570.

[15] G. De Martino, F. Pezzimenti, F.G. Della Corte, G. Adinolfi, G. Graditi, Design and numerical characterization of a low voltage power MOSFET in 4H-SiC for photovoltaic applications, in Proc. IEEE Int. Conf. Ph. D. Research in Microelectronics and Electronics - PRIME (2017) 221-224.

[16] F.G. Della Corte, G. De Martino, F. Pezzimenti, G. Adinolfi, G. Graditi, Numerical simulation study of a low breakdown voltage 4H-SiC MOSFET for photovoltaic module-level apllications, IEEE Trans. Electron Dev. 65 (2018) 3352-3360.

[17] H. Bencherif, L. Dehimi, F. Pezzimenti, A. Yousfi, Analytical model for the light trapping effect on ZnO:Al/c-Si/SiGe/c-Si solar cells with an optimized design, in Proc. of the 2018 International Conference on Applied Smart Systems, ICASS (2019) 8651990.

[18] F. Bouzid, F. Pezzimenti, L. Dehimi, F.G. Della Corte, M .Hadjab, A. H. Larbi, Analytical modeling of dual-junction tandem solar cells based on an InGaP/GaAs heterojunction stacked on a Ge substrate, J. Electron. Materials 48 (2019) 4107-4116.

[19] K. Zeghdar, L. Dehimi, F. Pezzimenti, S. Rao, F.G. Della Corte, Simulation and analysis of the current-voltage-temperature characteristics of Al/Ti/4H-SiC Schottky barrier diodes, Jpn. J. Appl. Phys. 58 (2019) 014002.

[20] H. Bencherif, L. Dehimi, F. Pezzimenti, G. De Martino, F.G. Della Corte, Multiobjective optimization of design of 4H-SiC power MOSFETs for specific applications, J. Electron. Mater. 48 (2019) 3871-3880.

[21] O. Manasreh, Semiconductor Heterojunctions and Nanostructures. Fayetteville, Arkansas: McGraw-Hill, lnc., 2005.

[22] S. Selberherr. Analysis and Simulation of Semiconductor Devices. Vienna, Austria: Springer, 1984.

[23] M.L. Megherbi, F. Pezzimenti, L. Dehimi, A. Saadoune, F.G. Della Corte, Analysis of the Forward I–V Characteristics of Al-implanted 4H-SiC p-i-n diodes with modeling of recombination and trapping effects due to intrinsic and doping-induced defect states, J. Electron. Mater. 47 (2018) 1414–1420.

[24] F. Bouzid, F. Pezzimenti, L. Dehimi, M.L. Megherbi, F.G. Della Corte, Numerical simulations of the electrical transport characteristics of a Pt/n-GaN Schottky diode, Jpn. J. Appl. Phys. 56 (2017) 094301.

[25] L. Sheng, S. Semiconductor Physical Electronics. Gainesville, Florida: Springer Science & Business Media, 2006.

[26] Y. Marouf, L. Dehimi, F. Pezzimenti, Simulation study for the current matching optimization in In0.48Ga0.52N/In0.74Ga0.26N dual junction solar cells, Superlattice. Microst. 130 (2019) 377-389.

[27] D. Guo, D. Vasileska, (2013, June). 1D fast transient simulator for modeling CdS/CdTe solar cells, in Proc. IEEE 39th Photovoltaic Specialists Conference, PVSC (2013) 1961-1965.

[28] D.B.M. Klaassen, A unified mobility model for device simulation-II. Temperature dependence of carrier mobility and lifetime, Solid-State Electron. 35 (1992) 961-967.

[29] M.L. Megherbi, F. Pezzimenti, L. Dehimi, M. A. Saadoune, F.G. Della Corte, Analysis of trapping effects on the forward current-voltage characteristics of Al-implanted 4H-SiC p-i-n diodes, IEEE Trans. Electron Dev. 65 (2018) 3371-3378.

[30] F. Pezzimenti, H. Bencherif, A. Yousfi, L. Dehimi, Current-voltage analytical model and multiobjective optimization of design of a short channel gate-all-around-junctionless MOSFET, Solid-State Electron. 161 (2019) 107642.

[31] H. Bencherif, L. Dehimi, F. Pezzimenti, F. G. Della Corte, Temperature and SiO2/4H-SiC interface trap effects on the electrical characteristics of low breakdown voltage MOSFETs, Appl. Phys. A-Mater. 125 (2019) 294.

https://doi.org/10.1016/j.ijleo.2019.164112

[32] H.P. Mahabaduge, W.L. Rance, J.M. Burst, M.O. Reese, D.M. meysing, C.A. Wolden, J. Li, J.D. Beach, T.A. Gessert, W.K. Metzger, S. Garner, T.M. Barnes, High-efficiency, flexible CdTe solar cells on ultra-thin glass substrates, Appl. Phys. Lett. 106 (2015) 133501.

[33] N. Amin, K. Sopian, M. Konagai, Numerical modeling of CdS/CdTe and CdS/CdTe/ZnTe solar cells as a function of CdTe thickness, Sol.Energ. Mat. Sol. C. 91 (2007) 1202-1208.

[34] M.W. Rahman, S.N. Ahmed, S.I. Rahman, Md. A. Hoque, Numerical analysis of CdTe thin film solar cells with CdS:O window layer and ZnO buffer layer, in Proc. IEEE International Conference on Advances in Electrical, Electronic and Systems Engineering - ICAEES (2016) 409-413.

[35] A. Haddout, A. Raidou, M. Fahoume, Influence of the layer parameters on the performance of the CdTe solar cells, Optoelectron. Lett. 14 (2018) 0098-0103.

[36] S. Khosroabadi, S.H. Keshmiri, Design of a high efficiency ultrathin CdS/CdTe solar cell using back surface field and backside distributed Bragg reflector, Opt. Express 22 (2014) A921-A929.

[37] J. Ma, D. Kuciauskas, D. Albin, R. Bhattacharya, M. Reese, T. Barnes, J. V. Li, T. Gessert, S.H. Wei, Dependence of the minority-carrier lifetime on the stoichiometry of CdTe using time-resolved photoluminescence and first-principles calculations, Phys. Rev. Lett. 111 (2013) 067402.

[38] G. Womack, P.M. Kaminski, J.M. Walls, Optical optimization of high resistance transparent layers in thin film cadmium telluride solar cells, Vacuum 139 (2017) 196-201.

[39] R.E. Treharne, A. Seymour-Pierce, K. Durose, K. Hutchings, S. Roncallo, D. Lane, Optical design and fabrication of fully sputtered CdTe/CdS solar cells, J. Phys. Conf. Ser. 286 (2011) 012038.